Journal of Non-Crystalline Solids 355 (2009) 2272–2278

Contents lists available at ScienceDirect

Journal of Non-Crystalline Solids

journal homepage: www.elsevier.com/locate/jnoncrysol

# Spin-coating of $Ge_{23}Sb_7S_{70}$ chalcogenide glass thin films

Shanshan Song [a], Nathan Carlie [b], Julie Boudies [b,c], Laeticia Petit [b], Kathleen Richardson [b], Craig B. Arnold [a,*]

[a] Department of Electrical Engineering and Princeton Institute for the Science and Technology of Materials, Princeton University, Princeton, NJ 08544, United States
[b] School of Materials Science and Engineering, COMSET, Clemson University, Clemson, SC 29634, United States
[c] Institut de Chimie de la Matière Condensée de Bordeaux, CNRS – Université Bordeaux 1, 87 Av. Dr. Schweitzer, 33608 Pessac, France

ARTICLE INFO

*Article history:*
Received 28 October 2008
Received in revised form 15 July 2009
Available online 26 August 2009

*PACS:*
42.70.Km
81.05.Kf

*Keywords:*
Spin-coating
Chalcohalides

ABSTRACT

Thin film $Ge_{23}Sb_7S_{70}$ chalcogenide glass has emerged as an important material system for photonic applications due to its high non-linear refractive index. However, one of the challenges is developing low-cost methods to deposit films of glassy material while retaining glass stoichiometry and high film quality. In this paper, we demonstrate a spin-coating technique for the deposition of such films. The dissolution mechanisms of $Ge_{23}Sb_7S_{70}$ in different solvents are studied in order to select the optimal solvent for film deposition. We show that the use of amine-based solvents allow the deposition of stoichiometric films in contrast to alkaline solutions. Films with low surface roughness (RMS roughness <5 nm) and controlled thickness (100–600 nm) can be deposited from solutions. We also show that annealing the films in vacuum decreases the amount of residual solvent, the presence of which is expected to lead to variation in optical properties of the thin films.



## 1. Introduction

Chalcogenide glasses are important low-loss mid-infrared materials [1] that exhibit a wide range of photo-induced phenomena and optical nonlinearities [2,3]. They are ideal candidates for various applications in infrared optics, such as optical discs, phase change memory, photolithography, holography, all-optical switching, laser written waveguides and photonic crystals [4–6]. In addition, the photosensitive properties of chalcogenide glasses enable optical tuning of photonic structures, such as tuning for solid-state lasers [7,8], photonic crystal waveguides [9] and cavities [10].

In particular, ternary chalcogenide Ge–Sb–S films have drawn attention for their high non-linear optical properties and compositional dependencies of various properties either within the Ge–Sb–S film system [11,12], or within the quaternary system Ge–Sb–S–Se realized by progressively replacing sulfur with selenium [13,14]. For example, with the substitution of S by Se in the Ge–Sb–S–Se system, the glass transition temperature decreases while the density increases, making optimization of the glass composition for specific applications possible.

Ge–Sb–S films in particular, and chalcogenide thin films in general, are conventionally prepared by vacuum coating techniques (thermal evaporation or sputtering) or pulsed laser deposition [15,16]. Whereas these are common approaches to thin film deposition, less conventional techniques such as spin-coating of glassy films from solution can have certain advantages for realizing large area, thick film, or localized material deposition [17]. For useful optical device manufacturing, it is important to retain the bulk glass stoichiometry in deposited thin films, since glass properties critically depend on material compositions [13]. In addition, obtaining high uniformity in refractive index, film thickness and low surface roughness requires careful optimization of the film deposition process.

Spin-coating of chalcogenide glass films is a low-cost, scalable method that provides additional flexibility in adding these important materials to existing devices. Chern and Lauks first introduced the spin-coating deposition method of preparing chalcogenide films in 1982 [17]. They demonstrated that amorphous chalcogenide films can be deposited from their solutions and retain many of the solute properties. Thermal, optical and structural properties of spin-coated $As_2S_3$ films deposited from propylamine or butylamine have been processed along with other binary chalcogenide systems (e.g., $As_2S_2$, $As_2Se_3$, $As_2Te_3$ and GeSe) [18,19]. Subsequent to these initial efforts, several groups have extended efforts to produce spin-coated chalcogenide films of $As_2S_3$, $As_2Se_3$ and $Sb_2S_3$ and investigated potential applications such as high-resolution photoresists and holographic gratings [20–23]. Spin-coating approaches have the added advantage that the same solutions can be adopted for other precision dispensing techniques such as ink jet or laser direct write [24,25], giving spatial control over the location of the added material with programmable patterns.

In this paper, the dissolution mechanism of the $Ge_{23}Sb_7S_{70}$ in different solvents is studied and compared as a function of the dissolution solvent. Glass film surface compositions are analyzed for films deposited from solutions with different solvents and

* Corresponding author. Tel.: +1 6092580250.
*E-mail address:* cbarnold@princeton.edu (C.B. Arnold).

0022-3093/$ - see front matter © 2009 Published by Elsevier B.V.
doi:10.1016/j.jnoncrysol.2009.07.015

glass/solvent ratios. We describe how the film deposition parameters can be optimized for depositing low surface defect films with good thickness uniformity and homogeneous optical properties. Lastly, we discuss the effect of the annealing on the amount of residual solvent in the film and its impact on the optical properties of the film.

## 2. Experimental

### 2.1. Bulk material preparation and film deposition

$Ge_{23}Sb_7S_{70}$ glasses and $As_2S_3$ glasses used as reference materials are prepared using a standard melting process described elsewhere [13]. The glasses are melted from high purity elements (As: Alfa-Aesar 99.999%, Ge: Sigma–Aldrich 99.999%, Sb: Alfa-Aesar 99.999% and S: Cerac 99.999%) which are weighed and batched inside a nitrogen-purged glove box and sealed using a gas–oxygen torch under vacuum into quartz ampoules at 100 °C. The ampoule is heated for 24 h to 800 or 925 °C, depending on composition. A rocking furnace is used to rock the ampoule during the melting process to increase the homogeneity of the melt. Once homogenized, the melt-containing ampoule is air-quenched and annealed at 40 °C below the glass transition temperature, $T_g$, for 15 h. Using energy-dispersive X-ray spectroscopy (EDS), the composition of the resultant bulk glass is found to be identical to the initial concentrations introduced in the batch.

Solutions of $Ge_{23}Sb_7S_{70}$ are prepared by dissolving bulk $Ge_{23}Sb_7S_{70}$ pieces into various solvents. The bulk glass samples are cut into $5 \times 5 \times 2$ mm blocks for weight loss measurements. In other cases, the bulk pieces are manually ground into a fine powder with sizes between 10 and 100 μm to increase the surface area and therefore to shorten the dissolution time. The dissolution is carried out inside a sealed glass container to prevent solvent evaporation. A magnetic stirrer is used to expedite the dissolution process. The resulting solution is stored inside a nitrogen-purged glove box, with less than 1 ppm of $O_2$ and $H_2O$, in order to eliminate possible sources of oxygen or water incorporation into solutions and subsequent films. The solution is then centrifuged at a speed of 3000 rpm for 3 min to remove any suspended or undissolved particulate or impurities [22]. One milliliter of the solution is pipetted onto the substrate, and the substrate is spun at 1000 rpm for 30 s. The resulting films are annealed in a nitrogen atmosphere at 90 °C for 1 h immediately after coating and then heated at 180 °C for 1 h in vacuum to remove excess solvent and to further densify the film. In this study, the investigated thin films of $Ge_{23}Sb_7S_{70}$ glass have been deposited onto either silicon wafers for energy-dispersive X-ray spectroscopy (EDS) and infrared spectroscopy, or onto glass microscope slides for optical spectroscopy and Zygo optical profilometry.

The surface composition of the films is examined using energy-dispersive spectroscopy (EDS) with a Hitachi model 3400 scanning electron microscope (SEM), equipped with an Oxford instruments EDS accessory. SEM micrographs and EDS spectra are obtained at 20 keV under variable pressure mode, typically at 30 Pa, in order to avoid sample charging. The surface profile of the films is measured with a Zygo Corp. *NewView 6300* white light interferometer microscope, under a 20× microscope objective and 0.5× zoom, giving a total magnification of 10× with an approximate resolution of 0.1 nm vertically and 1 μm laterally.

### 2.2. Dissolution kinetics and reaction order of chalcogenide glasses in solutions

Dissolution experiments on bulk glasses are conducted using aqueous solutions of potassium hydroxide (Alfa-Aesar, 50%), ammonium hydroxide (Aldrich, 30%), propylamine (Aldrich, 98%) or butylamine (Aldrich, 99.5%). The glass samples are first cut into $5 \times 5 \times 2$ mm rectangular blocks. Glass samples of known starting mass are immersed in solution and periodically removed for weight loss measurements to ascertain dissolution rate data. During the dissolution rate experiments, solution is left at ambient temperature and agitated with a magnetic stirrer at up to 800 rpm. The weight loss of a given sample is measured at 3–15 min intervals for up to 3 h depending on the solvent concentration. Based on these measurements, the dissolution rate $W$ (moles structure units/cm$^2$ s) is calculated using the following equation [26,27]:

$$W = \Delta m/(S \times M \times \Delta t), \tag{1}$$

where $\Delta m$ is the loss of weight (g), $S$ the total surface area of the initial bulk glass specimen (cm$^2$), $M$ the molecular weight of $AsS_{3/2}$ or $GeS_{4/2}$ and $SbS_{3/2}$ (g/mol) and $\Delta t$ the total lapsed time (s).

As the sample mass and surface area are kept constant, the variation of the dissolution rate (ChG + solvent → *products*) as a function of solvent (amine or hydroxide) concentration can be expressed as

$$W \propto C^n, \tag{2}$$

where $W$ is the dissolution rate defined above, $C$ the ionic concentration of the solvent (amine or hydroxide ion) in mol/L and $n$ the reaction order.

The reaction order with respect to the solvent can then be determined from the slope of the linear regression of the log–log plot,

$$\log(W) = n \cdot \log(C) + \log(k). \tag{3}$$

### 2.3. Optical properties measurement

The UV–Vis transmission spectra of the films are measured using an Ocean Optics HR4000 high-resolution spectrometer, whereas the infrared transmission spectra are measured with a Nicolet Fourier transform infrared (FTIR) spectrometer using a cooled mercury cadmium telluride (MCT) detector with a resolution of 4 cm$^{-1}$. Spectroscopic ellipsometry is also used to examine the refractive index. Ellipsometry is performed using a J.A. Woollam model M-44 spectroscopic ellipsometer which incorporates a variable angle stage allowing adjustment of the incident angle. The instrument operates on a rotating polarizer principle, in which the polarization of incoming light is varied, and reflected intensity is recorded with a grating coupled CCD over a wavelength range of 600–1100 nm. Thus, ellipsometric data was recorded at 55° and 75° angles of incidence, and data for both incident angles simultaneously fit with a Cauchy dispersion model using the instrument's software (WVASE32). The simultaneous fitting at multiple angles allows the simultaneous determination of both film thickness and refractive index dispersion.

## 3. Results

To be useful for device manufacturing, the spin-coated $Ge_{23}Sb_7S_{70}$ films are expected to have (i) composition similar to the bulk glass, (ii) low surface roughness (<5 nm) and (iii) uniformity in refractive index and thickness over the scale of a microscope slide. To achieve these requirements, the dissolution kinetics and reaction order of the glass have been studied as a function of different solvents and has been compared to those of the well-known $As_2S_3$ glass. Then we explain how to optimize the spin-coating process to deposit thin films which possess low surface roughness and good uniformity in thickness and refractive

index. Finally, we discuss the effect of the atmosphere during the film deposition process and the impact of annealing on the optical properties of the resulting film.

### 3.1. Dissolution kinetics and reaction order of chalcogenide glasses in solutions

It is well known that chalcogenide glasses can be dissolved in alkaline solution [28]. Borisova showed the chemical reaction at the glass surface is the rate-determining factor. The dissolution process for $As_2S_3$ glass in amine and hydroxide solutions has been well studied in recent years [29–32]; however the dissolution mechanism of $Ge_{23}Sb_7S_{70}$ glass remains unknown. A study of the dissolution mechanism of $Ge_{23}Sb_7S_{70}$ glass in different solvents reveals evidence of the glass' chemical stability and allows definition and selection of the optimal solvent for film deposition.

The dissolution rate of the $Ge_{23}Sb_7S_{70}$ glass when immersed in different solvents is determined by measuring glass weight loss as a function of immersion time. Fig. 1(a) shows the log of the dissolution rate $W$ as a function of log of amine or $OH^-$ concentration. It is observed that the dissolution rate of the glass when immersed in KOH at high concentrations (10 mol/L) is significantly higher than when immersed in $NH_4OH$ or other nitrogen-based solvents. The dissolution rates of the investigated glass when immersed in nitrogen-based solvents are similar within the experimental error of the measurements. The same experiments have been performed on $As_2S_3$ bulk glass specimens, which serve as a reference, and these results are shown in Fig. 1(b). One can notice that the $Ge_{23}Sb_7S_{70}$ glass dissolves with a similar rate as $As_2S_3$ when immersed in KOH but with a higher rate when immersed in $NH_4OH$ and a lower rate in propylamine and butylamine. We propose that this is due to the less covalent Ge–S bonds dominant in the ternary glass, as compared to the As–S bonds in $As_2S_3$. The lower bond strength and the difference between the two glasses suggest Ge–S bonds would be expected to dissolve faster in more polar solvent such as OH-based solution and slower in organic solvent such as amine.

The reaction orders are defined as the slope of the log $W$ as a function of log $C$. For both glasses, the reaction order of the glass when immersed in nitrogen-based solvents is approximately equal to zero, indicating that the solvent concentration has little or no effect on the dissolution rate. As seen previously [26], when the glasses are immersed in KOH, there appears to be a change in reaction order from approximately 1 to 0 when the $OH^-$ concentration increases. The dissolution mechanism of the glasses when immersed in KOH can be explained by a two-step dissolution through solid–solution interaction with an intermediate stage of adsorption of the reactant. This behavior is in agreement with previous observations for $As_2S_3$ [26,33] described by

$$OH^- + MS_{n/2} \leftrightarrow OH^- \cdots MS_{n/2} \quad \text{fast step}, \tag{4}$$

$$OH^- \cdots MS_{n/2} \leftrightarrow HO - M_{n-1/2} \quad \text{slow step}, \tag{5}$$

where M is either As or Ge depending on the composition, and $n$ the number of S atoms shared per unit (3 for As, 4 for Ge). The transition of the reaction order from 1 to 0 occurs at different KOH concentration for $As_2S_3$ and $Ge_{23}Sb_7S_{70}$ probably due to the slow step of the two-step process, which depends on the activation energy needed to break As–S or Ge–S bonds, thus leading to different dissolution rates. Also shown in Fig. 1 is the reaction order of the glasses when immersed in nitrogen-based solvents which is found to be independent of the concentration. In agreement with a previous study [33], this may indicate that the dissolution of the glass is controlled by the direct collision of high kinetic energy ammonium molecules or amine groups with the As atoms or Ge atoms at the surface of the glass. In this case, the molecules have low sensitivity to changes in the solvation layer at the glass surface, and thus are relatively unaffected by concentration, leading to a reaction order of zero with respect to the solvent concentration [34].

The composition of the glass surface after immersion in solvent has been analyzed using EDS coupled with a SEM. No surface composition variation of the $As_2S_3$ or $Ge_{23}Sb_7S_{70}$ glasses has been measured when the glasses were immersed in ammonium hydroxide, propylamine or butylamine. However, the analysis of the surface composition of the glasses when immersed in KOH reveals the presence of oxygen, the concentration of which was found to be dependent on the KOH concentrations as shown in Table 1. Oxygen was detected at the surface of the glasses only for high concentrations of KOH (>1 mol/L).

### 3.2. Film deposition

In order to deposit thin films with low surface roughness and good homogeneity of thickness and optical properties, the film deposition process has been optimized by examining the effects of the solvent, the glass to solvent ratio, the time elapsed during dissolution on the film composition, the effect of spin speed, and the annealing heat treatment.

#### 3.2.1. Solvents and glass to solvent ratio

Varying amounts of $Ge_{23}Sb_7S_{70}$ glass powder (0.25–2 g) have been dissolved for 48 h in propylamine and between 2 h and 2 weeks in $NH_4OH$. The composition of the resulting deposited

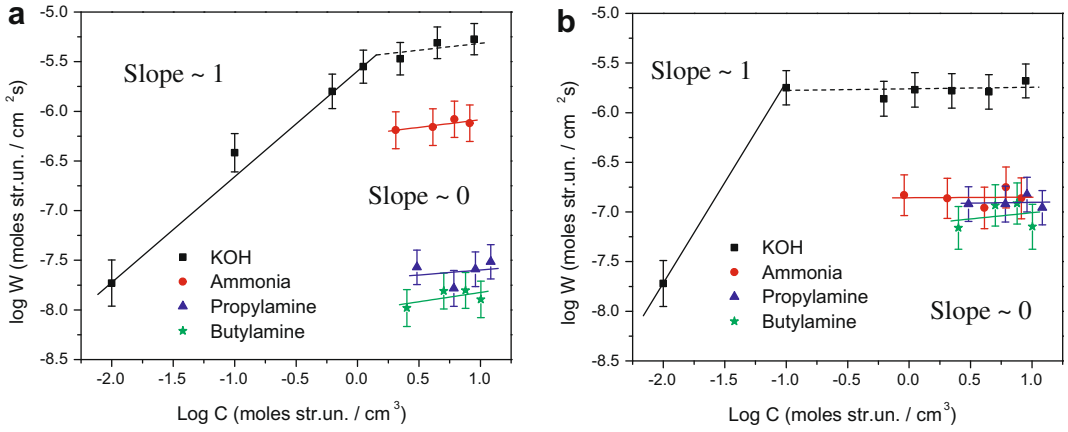


**Fig. 1.** Log–log plot of reaction rate ($W$) vs. concentration ($C$) for determination of reaction order, for (a) $Ge_{23}Sb_7S_{70}$ and (b) $As_2S_3$.

**Table 1**
EDS analysis of surface composition of $As_2S_3$ and $Ge_{23}Sb_7S_{70}$ bulk glasses after partial dissolution in various concentrations of KOH.

| KOH concentration (mol/L) | $As_2S_3$ surface composition (±2 at.%) | | | $Ge_{23}Sb_7S_{70}$ surface composition (±2 at.%) | | | |
|---|---|---|---|---|---|---|---|
| | As | S | O | Ge | Sb | S | O |
| 0.01 | 40 | 60 | 0 | 21 | 6 | 73 | 0 |
| 1 | 36 | 51 | 13 | 21 | 7 | 42 | 30 |
| 9 | 35 | 51 | 14 | 24 | 6 | 41 | 30 |

**Table 2**
EDS composition of films deposited from propylamine and $NH_4OH$ solutions with different glass to solvent ratio.

| Stirring duration | Concentration (g/10 mL) | % Ge (±2 at.%) | % Sb (±2 at.%) | % S (±2 at.%) |
|---|---|---|---|---|
| *Propylamine* | | | | |
| 6 h | 0.5 | 28 | 0 | 72 |
| 1 day | 0.5 | 26 | 3 | 71 |
| 2 days | 0.25 | 23 | 7 | 70 |
| 2 days | 0.5 | 24 | 6 | 70 |
| 2 days | 1 | 25 | 5 | 70 |
| 2 days | 2 | 29 | 0 | 71 |
| 5 days | 0.5 | 25 | 5 | 70 |
| *$NH_4OH$* | | | | |
| 2 h | 0.5 | 17 | 13 | 70 |
| 2 h | 1 | 11 | 15 | 74 |
| 2 weeks | 0.5 | 16 | 10 | 74 |
| 2 weeks | 1 | 5 | 10 | 85 |

films as measured by EDS are summarized in Table 2. When the glass is dissolved in 10 mL $NH_4OH$ for 2 h and for 2 weeks, the resulting films are deficient in Ge compared to the bulk. The concentration of Ge is even lower in films deposited from a highly concentrated solution (1 g of the glass in 10 mL of solution). When 0.25 g of glass is dissolved in propylamine for 2 days, the composition of the resulting film shows no deficiency or excess, corresponding to the composition of the parent bulk glass within the accuracy of the measurement. For larger amounts of glass dissolved in 10 mL of propylamine, the composition of the film is deficient in Sb. It is interesting to note that when 0.25 g of glass is dissolved in 10 mL of propylamine, no precipitate within the solution is observed and the solution maintains a green coloration during the experiment. When the mass of the glass increases to 0.5 g, a small amount of precipitation can be observed in the stirred solution. The dissolution of 2 g of glass leads to the presence of large amounts of reddish-brown particulate in the solution, which then gels into a dark red precipitate mass at the bottom of the vial below a light yellow layer of solution.

The dissolution duration of 0.5 g of glass in 10 mL of propylamine has been varied from 6 to 120 h. The films prepared from a solution stirred for 24 h or less are deficient in Sb while the films from a solution stirred for more than 2 days have similar composition to that of the bulk within the accuracy of the EDS measurement (±2 at.%).

As shown in Table 2, in order to deposit films with controlled composition and good stoichiometry, propylamine solvent is more appropriate than $NH_4OH$. As the film composition depends on solvent concentration and aging of the $NH_4OH$ solution, this fact makes $NH_4OH$ unsuitable for solvent-casting application despite its higher dissolution rate compared to amines. It is also observed that the composition of the film depends on the ratio between the mass of glass dissolved and the propylamine solvent and on the duration of the dissolution. The films from a solution of propylamine stirred for 24 h are deficient in Sb while the films from a solution stirred for more than 48 h have similar composition to that of the bulk within the accuracy of the EDS measurement.

As reported elsewhere [13], the glass network of $Ge_{23}Sb_7S_{70}$ is expected to be formed by $SbS_3$ pyramids and $GeS_4$ tetrahedral units along with a small number of $S_n$ chains and $S_8$ rings, due to the presence of excess sulfur. Based on Table 2, it is possible to think that the $GeS_4$ and S–S units are preferentially dissolved relative to $SbS_3$ units before saturation of the solution, as indicated by the deficiency in Sb for solutions with high concentration or short dissolution time. Therefore, to achieve a film composition similar to the bulk glass, the solution with a 0.5 g/10 mL glass to solvent ratio needs to be stirred for at least 48 h to fully dissolve the glass. Considering both ease of dissolving and composition consistency, propylamine has been found to be the most appropriate solvent in this study to dissolve the glass for the deposition of the films with controlled composition.

### 3.2.2. Spin-coating parameters

The spin-coating conditions have a significant influence on the surface quality of the films. The optical spectra of the films show a periodic variation of the transmission value as a function of wavelength, as shown in Figs. 2(b) and 3(b). This effect is caused by the interference between multiple reflections at the two surfaces of the film, and is influenced by both the film's thickness and its refractive index at that particular wavelength. We consider the resulting film to be of good uniformity of thickness and optical properties when the amplitude of the fringes is large and uniform.

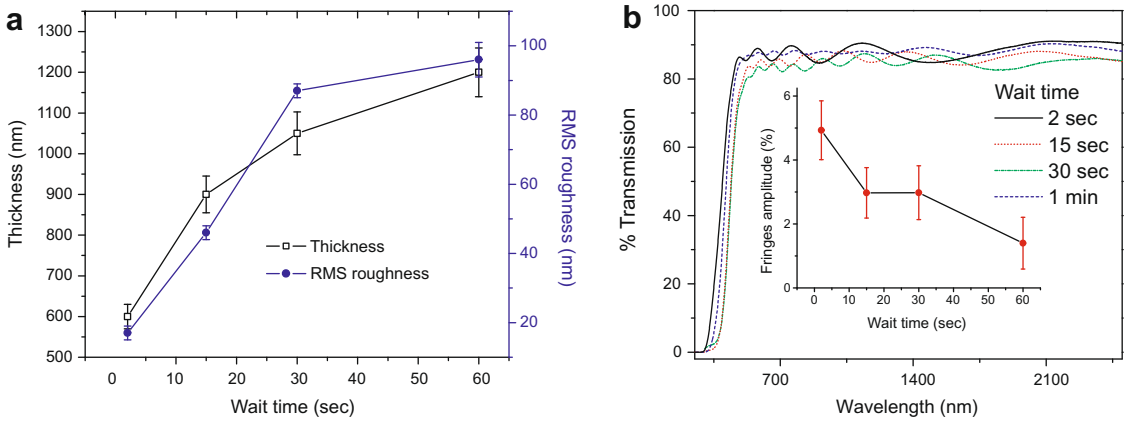


**Fig. 2.** Thickness and roughness measured by Zygo (a) and transmission spectra (b) of films prepared with different wait times prior to spinning; inset: average fringe amplitude. $Ge_{23}Sb_7S_{70}$ to propylamine ratio 0.5 g/10 mL, stirred for 48 h.

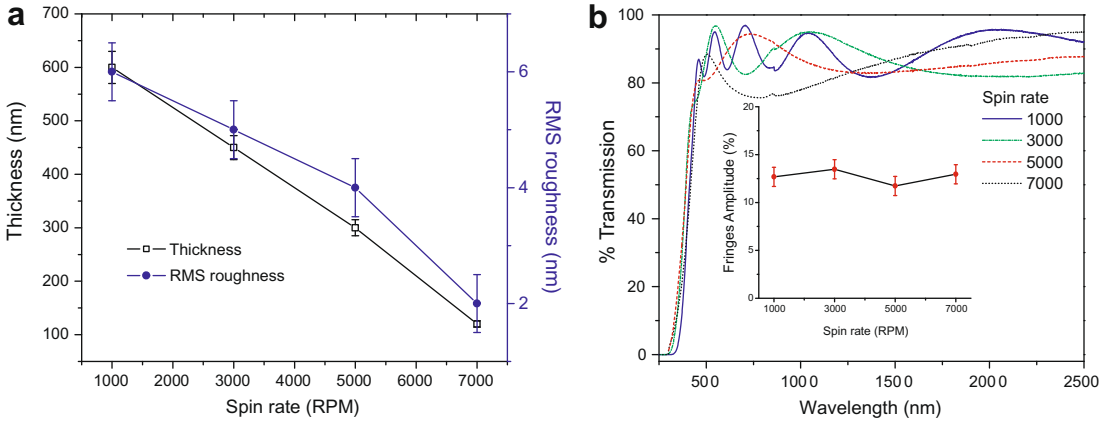


**Fig. 3.** Thickness and roughness measured by Zygo (a) and transmission spectra (b) of films prepared with different spin rates; inset: average fringes amplitude. $Ge_{23}Sb_7S_{70}$ to propylamine ratio 0.5 g/10 mL, stirred for 48 h.

It is interesting to note that a large spacing between fringes indicates a small film thickness.

The thickness and surface roughness of the films as a function of the wait time *before spinning* are shown in Fig. 2(a). When the wait time prior to spinning increases from 2 to 60 s, the resulting film thickness increases from 600 nm to about 1.20 μm (±5%) and the RMS roughness increases from approximately 20 to 100 nm (±2 nm). This is expected to be related to the partial evaporation of the solvent prior to the spinning. For longer wait times, the solution on the substrate will have higher viscosity, and therefore spreads out less under the centrifugal force of spinning leading to a thicker film. The transmission spectra of the resulting films are shown in Fig. 2(b). When the wait time increases, the amplitude of the fringes decreases, the uniformity of the fringe amplitude diminishes and the spacing between the fringes increases. These variations in the transmission spectra confirm the deposition of a thicker film as shown in Fig. 2(a) and also reveals an increase in film inhomogeneity (both thickness and optical properties) for longer wait times.

The effect of variation in spin rate on the surface quality of the thin films is shown in Fig. 3. Increasing spin rate from a minimum of 1000 up to 7000 rpm results in a decrease in film thickness from 600 to 120 nm (±5%). Film surface roughness varies from 6 to 3 nm (±0.5 nm) when the spin rate increases across the same range. This result is consistent with the increase in the spacing between the fringes in the transmission spectra observed when the spin rate increases as seen in Fig. 3(b). Furthermore, one can notice that the spin rate has no influence on the amplitude and uniformity of the transmission spectra fringes, indicating good uniformity in film thickness and optical properties. Figs. 2 and 3 clearly demonstrate the ability to deposit thin films with RMS roughness as low as 5 nm, and controlled and uniform thickness and optical properties.

### 3.2.3. Annealing conditions

FTIR is used to verify the presence of residual solvent in the films and the effects of film annealing. After spinning, the thin films are annealed at different temperatures for 1 h in order to evaporate residual propylamine in the film. The infrared transmission spectra of the resulting films are shown in Fig. 4(a). The spectra exhibit peaks between 2290 and 2380 $cm^{-1}$ which are related to the fluctuation of water and $CO_2$ levels in the uncontrolled atmosphere of the measurement chamber. The FTIR spectra also show an absorption band in the 2200–3200 $cm^{-1}$ range, the intensity of which decreases as the annealing temperature increases up to 180 °C. This absorption band can be assigned to N–H stretch and to aliphatic C–H stretches confirming the presence of residual solvent in the film annealed at 60 °C [18]. Annealing at higher temperature leads to an attenuation in these bands, indicating a decrease in the organic solvent content of the film. The films are found to free of organic content after an annealing at 180 °C in vacuum, as indicated by the disappearance of these bands in the spectra. The

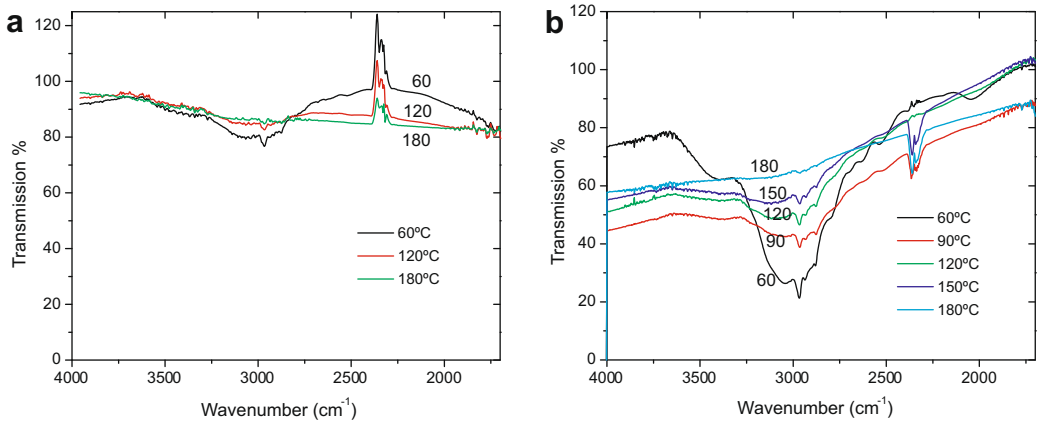


**Fig. 4.** Infrared transmission spectra of films spin-coated from solutions of $Ge_{23}Sb_7S_{70}$ in propylamine with different heat treatment: (a) prepared in $N_2$. Soft bake at 90 °C for 1 h, and then thermal anneal at 60, 120 and 180 °C for 1 h. Film thickness around 0.3 μm; (b) prepared in air. Soft bake at 60 °C for 1 h, and then thermal anneal at temperatures from 90 to 180 °C for 1 h. Film thickness is around 1.2 μm.

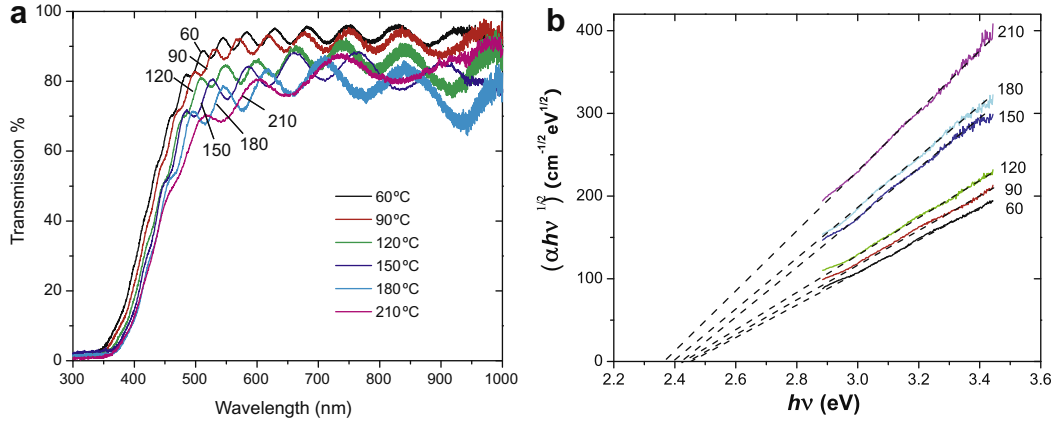


**Fig. 5.** (a) UV–Vis transmission spectra of spin-coated $Ge_{23}Sb_7S_{70}$ films from propylamine solution with different heat treatment prepared in air. (b) The dependence of $(h\nu)^{1/2}$ on photon energy ($h\nu$) in the films from which the effective optical band gap $E_g^{opt}$ is estimated (Tauc's extrapolation).

extent of minute amounts of residual organic has not been verified with other, more sensitive techniques.

To study the effects of atmosphere on the optical properties of the thin films, thin films are also prepared in ambient (air) atmosphere. We observe that the solutions prepared in air tend to produce more precipitate probably due to the presence of dissolved oxygen and water [22] present in the solvent used during the dissolution process. With the same dissolution and deposition conditions, the films prepared in air have similar composition and thickness to the films prepared in nitrogen-purged glove box. However, a larger surface roughness is measured for films prepared in the uncontrolled atmosphere most likely due to residual undissolved particulate or precipitates of oxide-containing residue. Films prepared in air have also been annealed in vacuum at different temperatures. Their infrared transmission spectra, which are similar to those of the films prepared in $N_2$ atmosphere, are shown in Fig. 4(b) and confirm the presence of residual solvent in the thin film which can be removed using heat treatment at high temperature. It is interesting to point out that the amplitudes of the absorption bands related to N–H and C–H in the spectrum of the film annealed at low temperature are larger when the film is prepared in air atmosphere as compared to a nitrogen atmosphere. The transmission spectra of these annealed films are shown in Fig. 5(a). When the annealing temperature increases, the amplitude of the fringes in the transmission spectrum of the film increases as well as the spacing between these fringes.

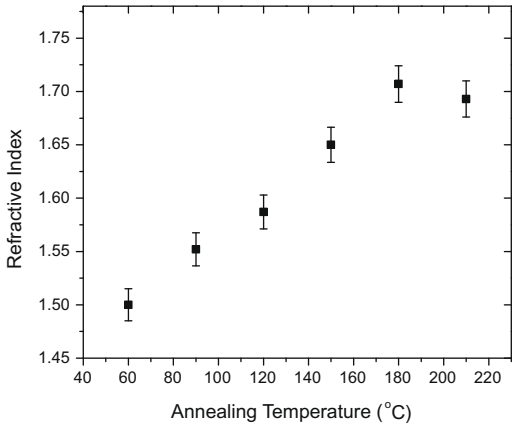


**Fig. 6.** Effect of post-soft bake annealing temperature on refractive index at 680 nm.

The optical band gap, $E_g^{opt}$ is determined from the absorption coefficient values using Tauc's extrapolation [35], i.e., from the relationship $\alpha(h\nu) = K\left(h\nu - E_g^{opt}\right)^2/h\nu$, where $K$ is a constant, and the optical band gap is defined as the intercept of the plot of $(\alpha h\nu)^{1/2}$ against $h\nu$. The effective band gaps of the films with residual solvent as a function of the annealing temperature are presented in Fig. 5(b). With increased annealing temperatures, there is a red-shift of the effective band edge. Using Swanepoel's method on the transmission spectra [36,37], the refractive index dispersion for the films are calculated and shown in Fig. 6 at 680 nm for different annealing temperatures. As seen in Figs. 5(a), (b) and 6, the loss of the solvent residue as well as the annealing treatment have a significant effect on the effective optical band edge and refractive index of the film. As expected, an increase of the annealing temperature was found to lead to the deposition of films with (i) lower thickness as seen by the progressive increase of the spacing between the fringes of Fig. 5(a), (ii) reduced effective band gap as seen in Fig. 5(b) indicating a higher relative permittivity and (iii) larger refractive index as seen in Fig. 6.

## 4. Discussion

Based on the above experiments in the $Ge_{23}Sb_7S_{70}$–propylamine system, the following conditions have been found to be optimal for depositing high quality films under 1 μm in thickness: (i) 0.5 g of ground bulk glass dissolved in 10 mL of propylamine; (ii) dissolution of glass for 48 h with constant stirring at 500 rpm; (iii) minimal wait time before spinning at speeds between 1000 and 3000 rpm; (iv) maintain the dissolution and coating processes under $N_2$ atmosphere and (v) soft-baking followed by annealing at 150–180 °C. Films deposited using the conditions defined above are further characterized by spectroscopic ellipsometry. The refractive index of the film at long wavelength $n(h\nu = 0)$ is found to be 2.02 ± 0.02, which is close to that of the bulk $Ge_{23}Sb_7S_{70}$ glass, measured at 2.21 ± 0.02 by ellipsometry [38].

## 5. Conclusions

In this paper, we demonstrate the successful deposition of stoichiometric films of $Ge_{23}Sb_7S_{70}$ using a spin-coating technique. The dissolution and spin-coating processes are optimized to achieve a low RMS surface roughness (<5 nm) film with uniform refractive index and thickness over large areas. Although only one composition is studied in this paper, the optimization process can be generalized to other chalcogenide glasses. The resulting film

quality for the glass composition examined is comparable to other techniques such as thermal evaporation and pulsed laser deposition [38], but with a lower cost and higher fabrication flexibility.

## References


[1] T. Kanamori, Y. Terunuma, S. Takahashi, T. Miyashita, J. Lightwave Technol. 2 (1984) 607.
[2] A.E. Owen, A.P. Firth, P.J.S. Ewen, Philos. Mag. B 52 (1985) 347.
[3] K. Petkov, P.J.S. Ewen, J. Non-Cryst. Solids 249 (1999) 150.
[4] A. Zoubir, M. Richardson, C. Rivero, A. Schulte, C. Lopez, K. Richardson, Opt. Lett. 29 (2004) 748.
[5] S. Wong, M. Deubel, F. Perez-Willard, S. John, G.A. Ozin, M. Wegener, G.V. Freymann, Adv. Mater. 18 (2006) 265.
[6] J.M. Harbold, F.O. Ilday, F.W. Wise, J.S. Sanghera, V.Q. Nguyen, L.B. Shaw, I.D. Aggarwal, Opt. Lett. 27 (2002) 119.
[7] T.K. Sudoh, Y. Nakano, K. Tada, Electron. Lett. 33 (1997) 216.
[8] S. Song, S.S. Howard, Z. Liu, A.O. Dirisu, C.F. Gmachl, C.B. Arnold, Appl. Phys. Lett. 89 (2006) 041115.
[9] M.W. Lee, C. Grillet, C.L.C. Smith, D.J. Moss, B.J. Eggleton, D. Freeman, B. Luther-Davies, S. Madden, A. Rode, Y. Ruan, Y. Lee, Opt. Exp. 15 (2007) 1277.
[10] A. Faraon, D. Englund, D. Bulla, B. Luther-Davies, B.J. Eggleton, N. Stoltz, P. Petroff, J. Vuckovic, Appl. Phys. Lett. 92 (2008) 043123.
[11] T. Asami, K. Matsuishi, S. Onari, T. Arai, J. Non-Cryst. Solids 226 (1998) 92.
[12] R. Vahalova, L. Tichy, M. Vlcek, H. Ticha, Phys. Status Solidi (A) 181 (2000) 199.
[13] L. Petit, N. Carlie, K. Richardson, Y. Guo, A. Schulte, B. Campbell, B. Ferreira, S. Martin, J. Phys. Chem. Solids 66 (2005) 1788.
[14] L. Petit, N. Carlie, R. Villeneuve, J. Massera, M. Couzi, A. Humeau, G. Boudebs, K. Richardson, J. Non-Cryst. Solids 352 (2006) 5413.
[15] V. Balan, C. Vigreux, A. Pradel, J. Optoelectron. Adv. Mater. 6 (2004) 875.
[16] K.E. Youden, T. Grevatt, R.W. Eason, H.N. Rutt, R.S. Deol, G. Wylangowski, Appl. Phys. Lett. 63 (1993) 1601.
[17] G.C. Chern, I. Lauks, J. Appl. Phys. 53 (1982) 6979.
[18] G.C. Chern, I. Lauks, A.R. McGhie, J. Appl. Phys. 54 (1983) 4596.
[19] G.C. Chern, I. Lauks, J. Appl. Phys. 54 (1983) 2701.
[20] B. Singh, G.C. Chern, I. Luaks, Appl. Phys. Lett. 45 (1984) 74.
[21] E. Hajto, P.J.S. Ewen, R.E. Belford, A.E. Owen, Thin Solid Films 200 (1991) 229.
[22] S. Shtutina, M. Klebanov, S.R.V. Lyubin, V. Volterra, Thin Solid Films 261 (1995) 263.
[23] T. Kohoutek, T. Wágner, Mir. Vlcek, M. Frumar, J. Non-Cryst. Solids 351 (2005) 2205.
[24] C.B. Arnold, A. Pique, MRS Bull. 32 (2007) 9.
[25] C.B. Arnold, P. Serra, A. Pique, MRS Bull. 32 (2007) 23.
[26] M.D. Michailov, S.B. Mamedov, S.V. Tsventarnyi, J. Non-Cryst. Solids 176 (1994) 258.
[27] S.B. Mamedov, M.D. Michailov, J. Non-Cryst. Solids 221 (1997) 181.
[28] Z.U. Borisova, Glassy Semiconductors, Plenum, New York, 1981.
[29] A. Kovalskiy, M. Vlcek, H. Jain, A. Fiserova, C.M. Waits, M. Dubey, J. Non-Cryst. Solids 352 (2006) 589.
[30] J. Orava, T. Wagner, M. Krbal, T. Kohoutek, M. Vlcek, M. Frumar, J. Non-Cryst. Solids 353 (2007) 1441.
[31] J. Orava, T. Wagner, M. Krbal, T. Kohoutek, M. Vlcek, M. Frumar, J. Non-Cryst. Solids 352 (2006) 1637.
[32] J.R. Neilson, A. Kovalskiy, M. Vlcek, H. Jain, F. Miller, J. Non-Cryst. Solids 353 (2007) 1427.
[33] M.R. Baklanov, S.M. Repinskii, Poverkhn. Fiz. Khim. Mekh. 3 (1984).
[34] E.A. Moelwyn-Hughes, Physical Chemistry, Pergamon, Oxford, 1961.
[35] J. Tauc, Mater. Res. Bull. 5 (1970) 721.
[36] R. Swanepoel, J. Phys. E 16 (1983) 1214.
[37] E. Marquez, J. Ramirez-Malo, P. Villarest, R. Jimenez-Garay, P.J.S. Ewen, A.E. Owen, J. Phys. D: Appl. Phys. 25 (1991) 535.
[38] N. Carlie, J. Hu, L. Petit, A. Agarwal, L.C. Kimerling, B. Luther-Davies, A.V. Rode, K. Richardson, in preparation.